Dynamic Evolution of the Surface Chemistry in Li^+-Conducting Membranes for Lithium Electrodeposition

[redacted]

Abstract

Solid polymer electrolytes (SPEs) are currently under investigation for their application as selective membranes for the transport of Lithium ions (Li^+) in electrochemical systems. In practice, this electrochemical feature can be used for economical Lithium electrodeposition, through transport of Li^+ between a low-cost anolyte and a highly polar Dimethyl Ether catholyte. However, few SPEs are insoluble in polar solvents, and the little information is available on the stability of said SPEs in electrolyte solutions.

In this work, we explore the changes in the surface chemistry of Polyacrylonitrile (PAN)-based and Poly(vinylidene fluoride -co-hexafluoropropylene) (PvDF-co-HFP)-based membranes in an electrodeposition cell. Each SPE was cycled in 1) an aqueous anolyte, consisting of a lithium carbonate-based solution, and 2) an organic catholyte, consisting of LiFSI and DME. Analysis of changes in the surface chemistry are is conducted using R-ray photoelectron spectroscopy (XPS).

Results of XPS analysis shows a carbonate layer forms on the surface of PAN:$LiClO_4$ and PvDF-co-HFP:LiFSI membranes in both catholyte and anolyte. Examinations of Cl2p and F2p spectra shows that $LiClO_4$ is prone to leaching in aqueous and DME electrolytes, and that LiFSI leaches into DME. Additionally, the presence of metallic fluoride, is confirmed after cycling PvDF-co-HFP:LiFSI in DME, suggesting LiX may be resistant to leaching. After further testing, LiBr is a possible Li salt replacement.

I. INTRODUCTION

As battery technology advances, the demand for inexpensive methods of manufacturing high quality Lithium metal electrodes increases[1,2]. To manufacture electrodes, a film of Lithium, on the order of 10 microns, must be deposited onto a substrate, such as a Copper current collector. Electrodeposition of Lithium represents an emerging process, yet this process requires tailored deposition solution to achieve a desirable thickness of Li metal.

Rather than undertaking the expense and additional waste of producing more deposition solution, the use of a specialized electrochemical cell with a selective membrane is proposed, which allows for Lithium cations to transfer from a cheap bulk anolyte to the catholyte, also known as the deposition solution (Figure 1). The anolyte is composed of Lithium salts dissolved in water, while the catholyte solution is composed of Li salts dissolved in Dimethoxyethane (DME), respectively.

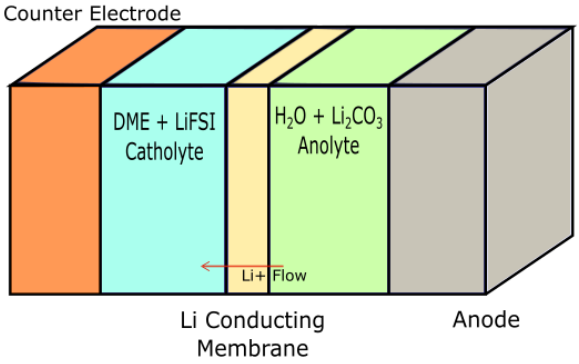

Figure 1 Electrodeposition cell. Contains Pt or SS anode, aqueous Lithium carbonate anolyte, dimethyl ether catholyte, and Cu counter electrode.

The performance of this system is limited by the ionic conductivity of the membrane, alongside its functional lifespan. This membrane material must have a high ionic conductivity, a minimum of 10^{-5} S/cm, and be chemically stable with the chosen anolytes and catholytes. Additionally, considerations must be made towards water-crossover, which can impact the deposition process.

Solid polymer electrolytes (SPEs), specifically polymer-in-salt electrolytes, are possible candidates for membranes in the aforementioned electrochemical cells. SPEs are easily formed into thin membranes using spray deposition or solution casting[3,4] and these membranes can possess ionic conductivities greater than 10^{-5} S/cm at room temperature.[3–10] However, it is unknown how repeated cycling in the proposed deposition cell will impact the SPEs structure and the ionic conductivity of the membrane as a result.

Two SPEs of interest are explored, Polyacrylonitrile (PAN) synthesized with $LiClO_4$ (PAN:$LiClO_4$), and Poly(vinylidene fluoride-co-hexafluoropropylene) -referred to as PvDF-co-HFP- synthesized with LiFSI (termed PvDF-co-HFP:LiFSI). PAN-based SPEs can reach ionic conductivities in the realm of 10^{-5} S/cm at room temperature[4–7,11,12]. Solution cast PvDF-co-HFP membranes are reported to reach 10^{-5} S/cm at room temperature, dependent on deposition temperature and wt. % of Li^+ source[9].

SPEs are prone to changes in surface chemistry during cycling[3,4,10,13,14]. These changes are well documented in Systems involving PEO or ether polymers, however relatively little is documented on the surface chemistry PAN and PvDF-co-HFP SPEs. It is known that changes in the surface chemistry of the selected SPEs occurs, but the specific changes and and source of said changes transformations is unknown. For the proposed system to be viable, a better understanding how SPEs interact with the anolyte and catholyte is required.

In this work, surface analysis and is used to characterize SPE candidates which have been cycled in anolyte and catholyte solutions. Samples are subject to electrochemical impedance spectroscopy to determine whether the ionic conductivity meets the minimum requirement. This information is then related to chemical phenomena at the surface, that in turn can impact the ability of these membranes to be used in emerging lithium electrodeposition technologies.

II. METHODS

A. Synthesis of Membranes

Polyacrylonitrile (PAN) membranes were formed using spray deposition. The spray solution was composed of PAN + $LiClO_4$ in a 2:1 mass ratio, and was dissolved into 50 mL of Dimethylformamide (DMF). The DMF solution was sprayed at a rate of 20 mL/hr with 5 bar of pressure onto a glass substrate placed on a hot plate. Filtered compressed air was used as the carrier gas. The apparatus was placed in a sealed chamber, and the temperature was kept between 90°C and 110°C.

PvDF-co-HFP membranes were formed using solution casting. Samples were composed of a 2:1 mass ratio of polymer and LiFSI dissolved in

Acetone. Casting was done on a glass substrate heated to 50°C on a hot plate.

After initial synthesis and analysis of the membranes, uncycled samples were aged for a minimum 14 days in the catholyte or anolyte solution. The anolyte was composed of 0.5 M Li_2CO_3 in an aqueous solution with added sulfuric acid to increase solubility of Li_2CO_3. The catholyte consisted of 1 M LiFSI with additives dissolved in 1,2-dioxymethane. After aging, XPS and EIS were conducted to determine changes in structure and ionic conductivity.

B. Apparatus

XPS analysis was conducted using a 180-degree hemispherical analyzer (ThermoFisher K-Alpha+), with an Al anode (*Al*-α, hv=1486.7 eV). A pass energy of 50.0 eV was used, and a step resolution of 0.1 eV. Accordingly, all binding energies are accurate to 0.1 eV. Normalization was conducted using adventitious carbon C1s at 284.8 eV.

Peak deconvolution was referenced to The *Handbook of X-ray Photoelectron Spectroscopy*[15] and Thermo Scientific Avantage XPS libraries.

III. RESULTS

A. PAN:$LiClO_4$

Peak binding energies (BE), Full Width at Half Maximum (FWHM) and at. % data for all PAN XPS spectra are contained in Appendix A. Any references to specific species in this text can be found in Appendix A. The same data for PvDF-co-HFP:LiFSI is contained in Appendix B.

Figure 2(b) shows the C1s spectra of PAN as the supplied precursor, uncycled membrane, and after cycling in the electrolyte solutions. Peaks were assigned for the precursor material to match the three unique carbon species present in PAN, whose monomer subunit is shown in fig. 1(a). The presence of a more electronegative species, Nitrogen, results in delocalization of electrons from the adjacent Carbons, resulting in Carbons closer to Cyanide having higher binding energies. The three deconvoluted peaks were initially symmetric and resembled previous works[16,17]. After spray deposition, symmetry was lost, and indicators of cyclization were found in the N1s and C1s regions. The enlarged peak at 297 eV is associated with development of Carbonates on the surface.

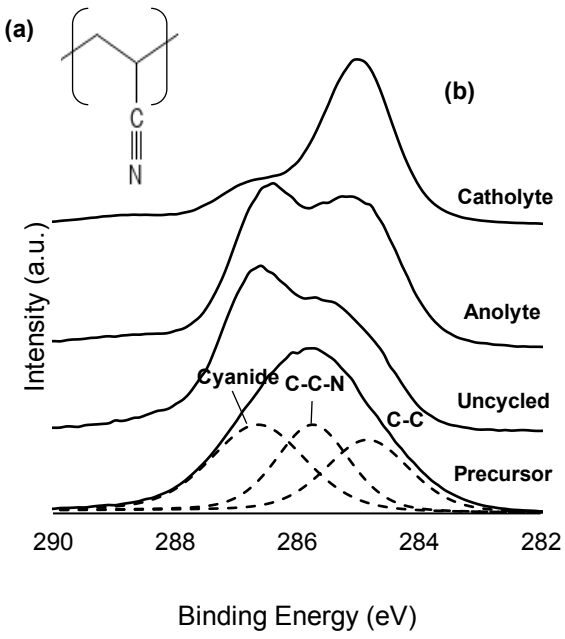

Figure 2 XPS analysis of the C1s region in PAN. (a) displays structure of PAN. (b) shows resulting curves and deconvolution of precursor material. Dashed curves are deconvoluted peaks and can be referenced to Appendix A.

The presence of cyanide was indicated by a consistent peak at 399.5 eV in the N1s spectra[15,17]. The intensity of the Cyanide peak increased after spray deposition and held constant during cycling. Changes in the intensity of cyanide is attributed to cyclization during spray deposition, consistent with the heat treatment of PAN in past works[16]. Additionally, the presence of different Nitrogen bonding motifs is seen at 398.9 eV, suggesting a highly limited degree of Nitrogen linking (~2 at. %). This linking raises concerns for water pass through. This assumption is further supported by an increased at. % of Ketone (C=O) at 532.3 eV in the uncycled sample.

The presence of $LiClO_4$ was confirmed after deposition by the presence of a small peak at 287.8 eV, attributed to the interaction between Carbon and the Oxygen in perchlorate. Peaks at 209 and 210 eV in the Cl2p spectra indicate Cl-O bonding motifs present in perchlorate.

Subsequent cycling in the anolyte led to the deposition of Carbonates onto the surface of PAN:$LiClO_4$. The O1s region, shown in fig. 3, develops a peak at 531.7 eV that was not present before cycling. The presence of this peak confirms development of a carbonate layer, assumed to be a

result of the deposition from the aqueous Li_2CO_3 anolyte. A corresponding increase in adventitious carbon contamination was experienced. A schematic for the deposition of Carbonate onto PAN:$LiClO_4$ is shown in fig. 4, where carbonate, from the aqueous Li_2CO_3 solution, interacts with the carbon of the Cyanide on PAN. This will explain the downshift in C1s nitrile peaks in fig. 1, the presence of C-O, and the increased intensity of the satellite above 290 eV. The Cl2p peaks at 209 and 210 eV, used to confirm the presence of Perchlorate, were reduced to less than 0.1 at. % after cycling in anolyte, alongside the Li1s. This confirms that $LiClO_4$ leeches into the anolyte.

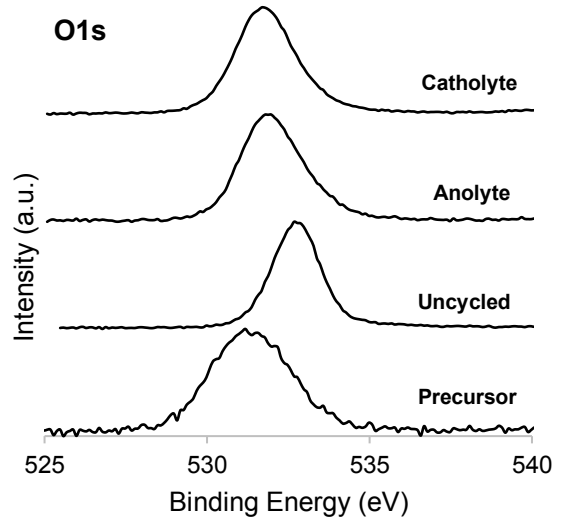

Figure 3 O1s spectrum of PAN determined using XPS. From top to bottom: Catholyte cycled, Anolyte cycled, uncycled, and precursor material.

The catholyte cycled sample had carbonate deposition present, alongside the direct presence C-O and C=O in the C1s and O1s spectrums. This is likely due to a reaction between to form surface hydroxyls on the polymer, which then react with CO_2 in air to form carbonates on the surface.

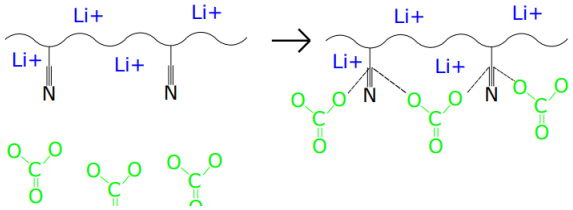

Figure 4 Proposed interaction between carbonate and surface of PAN. Presence of water in the solution allows for (reduction?) of Cyanide to NH to support slight aromaticity.

Additionally, a large percentage of organic chlorides were found, as indicated by the shift of the Cl2p from 209 and 210 eV to 198.8 and 200.4 eV. The source of organic chlorides is attributed to a reaction between DME and ClO_4. The relative amount of carbonate remaining on the surface is greater in the catholyte cycled sample, and the atomic mass fraction of Nitrogen dropped by 10%. Organic chlorides were found to have formed on the surface in the catholyte, denoted by a Cl2p3/2 peak at 198.8 eV, which is not present in any other treatment. This may be a result of reaction between DME and ClO_4^-. The formation of organic chlorides likely contributed to the lack of symmetry between peaks in the catholyte C1s of the catholyte cycled sample, were C-C bonds drowned out other signals. Overall, the catholyte cycled sample experienced a substantial change in surface chemistry caused by buildup of organic compounds on the surface due to undesired reactions. Accordingly, the presence of C-C increases by 37.6 at. %, and the presence of Cyanide decreases by 4.9 at. %, a factor of 4.6 and 2, respectively.

B. PvDF-co-HFP:LiFSI

The XPS spectra for C1s, F1s, O1s, and S2p of PvDF-co-HFP are shown in fig. 5 (a)-(d). The uncycled film shown in (a)-I and (a)-II reflects all expected carbon species from PvDF-co-HFP.

The initial precursor shows a small presence of the fluorinated carbons expected upfield of 290 eV. This is a result of heavy carbonate deposition, likely in direct interaction with deshielded fluorinated carbons. Solution casting removes the surface carbonate layer, leading to substantial expression of CF, CF_2, and CF_3 peaks, detailed in Appendix B. A small presence of metallic fluoride, presumed to be from coordination between a Ca contaminant and Fluorine, was removed during casting. The Calcium is presumed to be a catalyst in the product of PvDF-co-HFP. Confirmation of the presence of LiFSI in PvDF-co-HFP:LiFSI is done through the S2p spectra. Comparison of the pure LiFSI peak in fig. 5 (d) shows that FSI is not actively participating in bonding.

Cycling in anolyte did not result in leching of LiFSI, with the at. % of LiFSI increasing to 3.13. The C1s spectra shows a presence of carbonates at 288.4 eV, due to deposition of carbonate from the Li_2CO_3 solution. This results in a drop in the

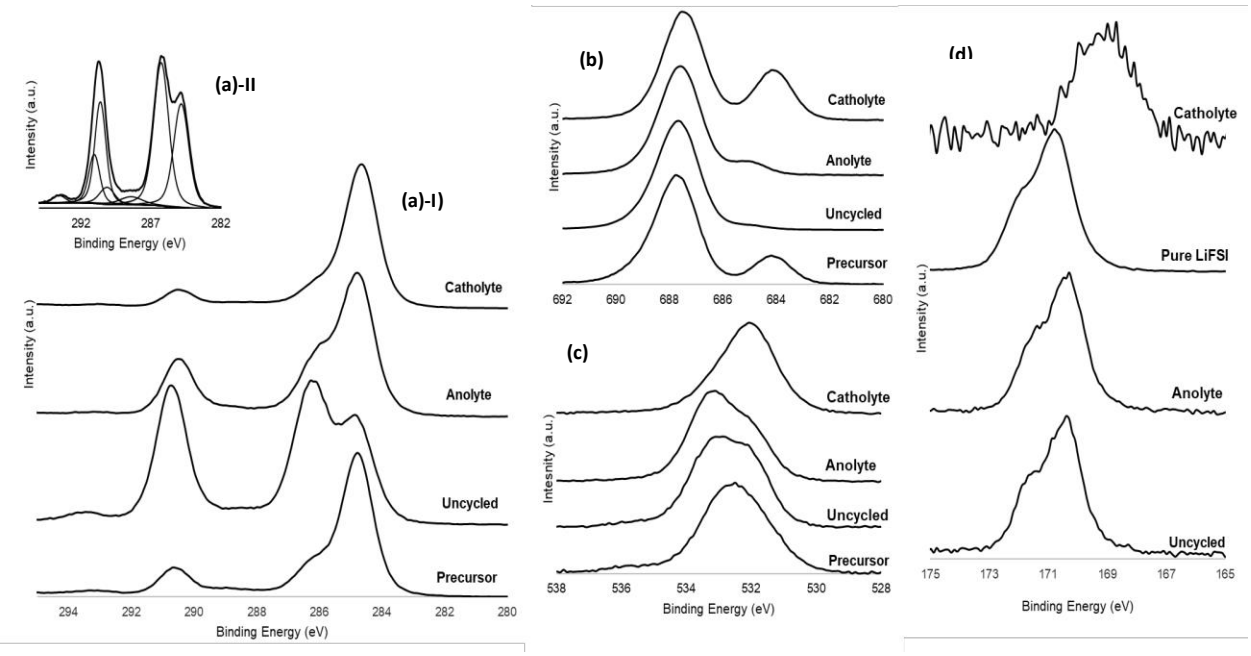

Figure 5 XPS spectra of PvDF-co-HFP. Comparison of C1s spectra (a)-I. Deconvolution for uncycled sample (a)-II. (b) Displays F1s spectra comparison, (c) refers to O1s, and (d) displays S2p. All curves are scaled from 0 to 1 to reflect semi-quantitative measurements. Breakdown of peaks in (a)-II is included in table 1. CF3 peak present in Uncycled C1s is not present beyond .01 at. % in any other samples.

presence of fluorinated carbons, which results from surface contaminants drowning out the presence of C-F. However, The presence of organic Fluorine species did not decrease substantially during cycling, remaining at or below 35 at. %. It is difficult to differentiate different fluorine bonds in the F1s spectra due to differences in binding energy being less than .2 eV (Cite Avantage DB), therefore changes in specific F-C bonding motifs cannot be described. A noteworthy development is the presence of a slight peak at 685 eV, attributed to coordination between Li and F.

The catholyte cycled sample shows signs of more thorough adventitious carbon deposition on the surface. However, the presence of carbonate peaks is minimal compared to the development of C-O bonding on the surface. This results from an interaction between PvDF-co-HFP and DME, such that DME binds on the surface, accounting for the ether bonds. As a result, the C1s spectrum of the catholyte cycled PvDF-co-HFP:LiFSI greatly resembles the precursor PvDF-co-HFP. The presence of metallic fluorides experienced a large uptick after cycling in DME, reaching 13.1 at. %. This includes the possibility of LiF formation, and stability of LiF in the catholyte. Analysis of the S2p spectrum shows a stark drop in at. %, becoming unreadable. LiFSI in leaches into DME rapidly. This contrasts to the formation of metallic fluorides, which appear to be resistant to leaching in DME.

IV. Conclusions

As shown in this report, both PAN and PvDF-co-HFP are stable in aqueous Li_2CO_3 anolytes as well as DME based catholytes. In both cases carbonates form on the surface of the membranes, but the effect is less sever in PvDF-co-HFP:LiFSI. It is recommended that PvDF-co-HFP is utilized as the polymer matrix moving forwards, due to its greater stability, and resemblance to the precursor state when cycled in DME. However, the ionic conductivity of the PvDF-co-HFP electrolytes will require further improvement for such membranes to enable fast Lithium electrodeposition.

However, it was determined that both $LiClO_4$ and LiFSI leached into DME, reducing the functional lifespan of the membrane. Additionally, it DME appears to dissolve Li^+ from the surface of the membrane. For these reasons, neither Li salt is recommended, and a an alternative salt must be found in order to increase the membrane lifespans while minimizing possible water crossover in the membranes.

In subsequent work, LiBr will be tested as an alternative to LiFSI and $LiClO_4$. Coordination between F and metallic Li was found when testing the PvDF-co-HFP membrane in DMOE, and suggests Lithium Halide salts may be insoluble in the catholyte solution. Additionally, the smaller size of halides may reduce the degree of water crossover in the event LiX is leached from the surface.

V. Acknowledgements

This work was supported in part by the U.S. Department of Energy, Office of Science, Office of Workforce Development for Teachers and Scientists (WDTS) under the Science Undergraduate Laboratory Internships (SULI) program.

Appendix 1: XPS Data for PAN:$LiClO_4$

Precursor				Uncycled				Anolyte				Catholyte			
Peak BE (eV)	FWHM (eV)	Atom %	Species	Peak BE (eV)	FWHM (eV)	Atom %	Species	Peak BE (eV)	FWHM (eV)	Atom %	Species	Peak BE (eV)	FWHM (eV)	Atom %	Species
284.84	1.64	22.09	**C**-C	208.2	1.26	2.25	Perchlorate	55.33	2.16	2.68	LiCl	198.78	1.31	6.12	Organic Chloride
285.73	1.43	23.05	**C**-C-N	209.86	1.17	---	Perchlorate	199.75	3.51	0.07	Cl2p	200.42	1.31	---	Organic Chloride
286.63	1.85	29.98	Cyanide, C=**O**	284.83	1.39	10.3	C-C	207.48	1.02	0.04	Cl2p	283.42	0.75	1.34	Carbide
398.82	1.72	19.47	Cyanide	285.65	1.43	16.02	Cb	284.77	1.25	26.32	C-C	284.84	1.22	48	C-C
399.68	1.24	1.67	Organic Matrix	286.72	1.19	19.27	Cy	285.5	0.91	10.71	Cb	285.46	0.91	9.59	Cb
530.96	2.38	2.65	C-**O**	287.81	2.02	4.29	C=O or C-Cl	286.49	1.27	34.25	Cy	286	0.72	4.63	C-O
532.29	2.16	1.09	C=**O**	398.9	1.51	0.64	C=**N**-C	288.96	2.08	2.35	C=O	286.7	0.91	9.6	Cy
				399.81	1.21	10.72	Cyanide	399.54	1.2	14.8	Cyanide	287.38	0.78	2.39	C-Cl
				401.14	1.77	1.09	Organic Matrix	531.72	1.77	6.27	C-O	288.72	1.58	3.49	Carbonate
				532.73	1.75	33.97	Perchlorate, C=**O**	532.87	1.97	2.5	C=O, C-Cl	399.76	1.28	5.82	Cyanide
				535.5	2.35	1.45	**O**-Fx					531.64	1.86	7.48	C-O
												532.83	1.9	1.54	C=O

Appendix II: XPS Data for PvDF-co-HFP:LiFSI

Precursor				Uncycled				Anolyte				Catholyte			
Peak BE (eV)	FWHM (eV)	Atom %	Species	Peak BE (eV)	FWHM (eV)	Atom %	Species	Peak BE (eV)	FWHM (eV)	Atom %	Species	Peak BE (eV)	FWHM (eV)	Atom %	Species
284.62	0.9	7.63	C-C	56.59	0.58	1.03	LiFSI	56.01	1.5	3.9	Li1s LiFSI	169.06	2.55	0.14	FSI
284.84	1.25	31.26	C-C	170.37	1.38	1.76	FSI	170.27	1.35	3.13	FSI	284.3	0.98	9.46	SP2
286.2	1.2	7.57	CH2-CF2	171.47	1.38	---	FSI	171.44	1.35	0	FSI	284.76	1.01	20.43	SP3
289.01	1.63	1.76	C=O	284.82	1.29	13.4	C-C	284.09	0.79	0.71	SP2	285.74	1.64	7.8	C-N or C-S or C-O
290.25	0.76	2.21	CF2-CH	286.25	1.27	18.36	C-S or C-N or C-O	284.76	1.16	26.19	SP3	288.61	2	1.21	C=O
290.57	0.54	1.09	CF2-CF-CF3	288.41	1.86	1.43	C=O	285.83	1.24	8.86	C-N or C-S	289.92	0.72	0.49	CF2-CH
290.91	0.76	2.68	CF-CF3	290.13	1.27	2.21	CF2-CH	286.35	1.16	4.06	C-O	290.33	0.66	1.21	CF2-CF-CF3
293.27	1.03	0.56	CF3	290.61	0.94	9.72	CF2-CF-CF3	289.07	2.08	2.31	Carbonate	290.75	0.72	1.32	CF-CF3
295.62	0.83	0.11	Satellite	291.05	0.94	4.63	CF-CF3	290.01	0.72	2.02	CF2-CH	399.87	3.05	0.19	C-NH2, Cyanide
406.98	6.26	3.23	Nitrate	293.56	1.04	0.8	CF3	290.47	0.69	4.68	CF2-CF-CF3	406.94	1.5	0.22	Nitrate
531.61	1.66	1.83	C-O	531.97	1.54	2.85	FSI	290.92	0.71	2.48	CF-CF3	531.7	1.58	5.95	C=O
532.76	1.91	5.18	C=O	533.24	1.65	3.76	C=O	293.26	0.74	0.13	CF3	532.19	1.05	1.37	S=O
535.63	1.36	0.17	O-Fx	687	1.01	10.16	F1s A	400.03	1.46	1.75	C-NH2, Cyanide, Matrix	532.85	1.83	4.61	Nitrate
684.12	1.59	16.14	Metallic Fluoride	687.64	0.9	14.09	F1s B	531.97	1.39	3.37	C=O	684.09	1.61	13.08	Metallic Fluoride
687.61	1.6	14.05	CF3	688.3	1.09	12.69	F1s C	533.26	1.57	7.09	S=O	687.48	1.79	32.5	C-F
688.61	1.82	4.53	CF2	689.18	1.31	3.12	F1s C-F	684.95	1.24	1.71	LiF or SiF				
								687.63	1.84	27.61	C-F				

References

[1] D. Lin, Y. Liu, and Y. Cui, Nature Nanotechnology **12**, (2017).

[2] M. Balaish, J.C. Gonzalez-Rosillo, K.J. Kim, Y. Zhu, Z.D. Hood, and J.L.M. Rupp, Nature Energy **6**, (2021).

[3] M. Li, C. Wang, Z. Chen, K. Xu, and J. Lu, Chemical Reviews **120**, 6783 (2020).

[4] L. Long, S. Wang, M. Xiao, and Y. Meng, Journal of Materials Chemistry A **4**, 10038 (2016).

[5] H.S. Min, J.M. Ko, and D.W. Kim, in *Journal of Power Sources* (2003), pp. 469–472.

[6] Y. Chen-Yang, H. Chen, F. Lin, and C. Chen, *Polyacrylonitrile Electrolytes 1. A Novel High-Conductivity Composite Polymer Electrolyte Based on PAN* (n.d.).

[7] K.M. Abraham and M. Alamgir, Journal of The Electrochemical Society **137**, 1657 (1990).

[8] P. Raghavan, X. Zhao, J.K. Kim, J. Manuel, G.S. Chauhan, J.H. Ahn, and C. Nah, Electrochimica Acta **54**, 228 (2008).

[9] M. Abreha, A.R. Subrahmanyam, and J. Siva Kumar, Chemical Physics Letters **658**, 240 (2016).

[10] Y. Zhao, Y. Bai, W. Li, M. An, Y. Bai, and G. Chen, Chemistry of Materials **32**, 6811 (2020).

[11] H. Xu, X. Zhang, J. Jiang, M. Li, and Y. Shen, Solid State Ionics **347**, 115227 (2020).

[12] X. Wang, Y. Fang, X. Yan, S. Liu, X. Zhao, and L. Zhang, Polymer **230**, 124038 (2021).

[13] L. Grande, E. Paillard, J. Hassoun, J.B. Park, Y.J. Lee, Y.K. Sun, S. Passerini, and B. Scrosati, Advanced Materials **27**, 784 (2015).

[14] J.B. Goodenough and Y. Kim, Chemistry of Materials **22**, 587 (2010).

[15] J.F. Moulder, W.F. Stickle, P.E.' Sobol, K.D. Bomben, and J. Chastain, *Handbook of X-Ray Photoelectron Spectroscopy AReference Book of Standard Spectra for Identification and Interpretation of XPS Data* (n.d.).

[16] C.R. Wu, W.R. Salaneck, J.J. Ritsko, and J.-L. Bredas, *X-RAY PHOTOELECTRON SPECTROSCOPY OF POLYACRYLONITRILE* (1986).

[17] T. Takahagi, I. Shimada, M. Fukuhara, " K Morita, and A. Ishitani, *XPS Studies on the Chemical Structure of the Stabilized Polyacrylonitrile Fiber in the Carbon Fiber Production Process* (n.d.).